Available online at www.sciencedirect.com

ScienceDirect

Geochimica et Cosmochimica Acta 214 (2017) 14–29

Geochimica et Cosmochimica Acta

www.elsevier.com/locate/gca

Fe-periclase reactivity at Earth's lower mantle conditions: *Ab-initio* geochemical modelling

Marcello Merli [a], Costanza Bonadiman [b], Valeria Diella [c], Luciana Sciascia [a], Alessandro Pavese [d,e,*]

[a] *Department of Earth and Marine Sciences, University of Palermo, Via Archirafi 36, 90123 Palermo, Italy*
[b] *Department of Physics and Earth Sciences, University of Ferrara, Via Saragat 1, 44122 Ferrara, Italy*
[c] *Consiglio Nazionale delle Ricerche, CNR-IDPA, Sezione di Milano, Via Botticelli 23, 20133 Milano, Italy*
[d] *Department of Earth Sciences "A. Desio", University of Milan, Via Botticelli 23, 20133 Milan, Italy*
[e] *Department of Earth Sciences, University of Turin, Via Valperga Caluso 35, 10100 Turin, Italy*

Received 25 August 2016; accepted in revised form 14 July 2017; available online 28 July 2017

Abstract

Intrinsic and extrinsic stability of the (Mg,Fe)O solid mixture in the Fe-Mg-Si-O system at high *P*, *T* conditions relevant to the Earth's mantle is investigated by the combination of quantum mechanical calculations (Hartree- 26 Fock/DFT hybrid scheme), cluster expansion techniques and statistical thermodynamics. Iron in the (Mg,Fe)O binary mixture is assumed to be either in the low spin (LS) or in the high spin (HS) state. Un-mixing at solid state is observed only for the LS condition in the 23–42 GPa pressure range, whereas HS does not give rise to un-mixing. LS (Mg,Fe)O un-mixings are shown to be able to incorporate iron by subsolidus reactions with a *reservoir* of a virtual bridgmanite composition, for a maximum *total* enrichment of ~0.22 FeO. At very high *P* (up to 130/3150 GPa/K), a predominant (~0.7 phase proportion), iron-rich Fe-periclase mixture $(Mg_{0.50}Fe_{0.50})O$ is formed, and it coexists, at constrained phase composition conditions, with two iron-poor assemblages [$(Mg_{0.90}Fe_{0.10})O$ and $(Mg_{0.825}Fe_{0.175})O$]. These theoretical results agree with the compositional variability and frequency of occurrence observed in lower mantle Fe-periclase from diamond inclusions and from H*P*-H*T* synthesis products. The density difference among the Fe-periclase phases increases up to ~10%, between 24 and 130 GPa. The calculated bulk Fe/Mg partitioning coefficient between the bridgmanite *reservoir* and Fe-periclase, Kd, is 0.64 at 24 GPa; it then drops to 0.19 at 80 GPa, and becomes quasi-invariant (0.18–0.16) in the lowermost portion of the Earth's mantle (~80–130 GPa). These Kd-values represent an approximate estimate for the Fe/Mg-partitioning between actual bridgmanite and Fe-periclase. Consequently, our Kd-values agree with experimental measurements and theoretical determinations, hinting that iron preferentially dissolves in periclase with respect to all the other iron-bearing phases of the lower mantle. The continuous change up to 80 GPa (~2000 km depth) of the products (compositions and phase proportions) over the MgO-FeO binary causes geochemical heterogeneities throughout the lower mantle, but it does not give rise to any sharp discontinuity. In this view, anomalies like the ULVZs, explained with a local and abrupt change of density, do not seem primarily ascribable to the mixing behavior and reactivity of (Mg,Fe)O at subsolidus.

Keywords: MgO-FeO binary; Pyrolitic geochemical model; Lower mantle geochemical heterogeneities; Subsolidus reaction modelling; Mixing Gibbs energy

* Corresponding author at: Department of Earth Sciences, University of Turin, Via Valperga Caluso 35, 10100 Turin, Italy.
E-mail address: alessandro.pavese@unito.it (A. Pavese).

http://dx.doi.org/10.1016/j.gca.2017.07.030
0016-7037/

1. INTRODUCTION

1.1. (Mg,Fe)O-system

The Earth's lower mantle is home to some of the most fascinating problems related to the interior of our planet, ranging from sharp discontinuity to anisotropy and unresolved geochemical processes, *i.e.* origins of mantle plumes, segregation of dense sub-ducted slab components, residual of core formation processes and core/mantle chemical exchange (Albarede and van der Hilst, 2002).

All the Earth Reference models (*e.g.* PREM and AK135; Dziewonski and Anderson, 1981; Kennett et al., 1995), which are designed to match whole Earth mechanical properties and astrophysical data, agree to indicate Fe-periclase and (Mg,Fe)-perovskite (bridgmanite) as the main phases of the lower mantle bulk phase-composition. Therefore, the reactions involving the subsolidus MgO-FeO system (*i.e.* Fe-periclase phase) provide a relevant contribution to the general geochemical behaviour of the lower mantle. Seismic anomalies are associated to geochemical discontinuities, such as those of the D″-layer (Lay and Helmberger, 1983; Sidorin et al., 1999; Kaneshima and Helffrich, 1999; Murakami et al., 2012) and ULVZs (McNamara et al., 2010), in the lowermost portion of the Earth's mantle. Geochemical perturbations in this region are ascribed to diverse possible causes, some of which are related to the Fe content and its distribution in the lower mantle phases, *i.e.*: (i) high-to-low spin state transition of iron in Fe-periclase (Dobson and Brodholt, 2005; Mao et al., 2006; Lin et al., 2013; Zhang et al., 2016); (ii) appearance of new phases, *e.g.* a post-perovskite, Fe-segregation in iron-bearing phases, Si-Mg-Fe melts and partially molten systems (Trampert et al., 2004; Murakami et al., 2005, 2012; da Silva et al., 2000; Karki et al., 2001; Wentzcovitch et al., 2004; Garnero, 2004; Lay et al., 2004; Nomura et al., 2011; Andrault et al., 2011; Thorne et al., 2013; Zhang et al., 2016).

Although the (Mg,Fe)O solid mixture at high pressure and high temperature conditions (H*P*-H*T*) has been largely investigated (*e.g.*: Vassiliou and Ahrens, 1982; Richet et al., 1989; Fei et al., 1992; Dubrovinsky et al., 2000, 2001; Kung et al., 2002; Jacobsen et al., 2004; Zhang and Kostak, 2002; van Westrenen et al., 2005; Jackson et al., 2006; Lin et al., 2009), several questions are still open, *i.e.* the un-mixing process and the highest allowed Fe content in the lower mantle Fe-periclase. Some authors (*e.g.*: Lin et al., 2003; Ohta et al., 2014) do not observe un-mixing of (Mg,Fe)O in static compression experiments, whereas others (Dubrovinsky et al., 2000, 2001) report a gradual formation of magnesium-rich and iron-rich oxide phases from (Mg,Fe)O at *P* and *T* above 80 GPa and about 1000 K, respectively. In addition, Fe-periclase obtained by H*P*-H*T* Fe/Mg partitioning experiments from a starting material bearing 0.1–0.3 FeO (Auzende et al., 2008; Sinmyo et al., 2008; Nakajima et al., 2012; Prescher et al., 2014) shows a wide compositional range (0.088–0.487 FeO) with respect to the coexisting (Mg,Fe)-perovskite (0.026–0.161 FeO). These results are in keeping with observations of lower mantle Fe-periclase findings (~0.15–0.70 FeO) that occur as inclusions in diamonds (Kaminsky, 2012 and reference therein). It is worth noting that ~0.3–0.5 FeO natural compositions (Kaminski, 2012) have a relevant statistical occurrence (55 out of 230 samples), whereas Mg-wüstite (0.5–0.7 FeO) is rarely observed (6 out of 230 samples). Such a variety, in terms of Fe-periclase compositions, is difficult to be explained in the frame of the extant experimental works on un-mixing processes (*i.e.* Ohta et al., 2014 and reference therein). All this has led some authors (Javoy et al., 2010; Kaminsky, 2012) to ultimately invoke a different reference Earth model (enstatite/chondrite *versus* pyrolite) to account for the bulk lower mantle composition (Badro et al., 2003; Mao et al., 2006; Matas et al., 2007; Irifune et al., 2010).

In this work the miscibility of (Mg,Fe)O and possible disequilibrium reactions with a *reservoir*, which complements the Fe-periclase in the formation of the bulk lower mantle, are investigated and the results of our study are compared with observations.

The bulk lower mantle was split into two different geothermal regions: the lower mantle (LM) and the lowermost lower mantle (LLM). LM accounts for the mantle region well below the transition zone (>23 GPa; >700 km) and above the perturbed D″-layer, and exhibits relatively smooth trends of seismic profiles. In this view, LM can be considered as a seismically and chemically homogeneous lower mantle portion, along a given model geotherm. LLM, in turn, refers to the lowermost region of the Earth's mantle (>80 GPa; >2000 km), where deviations in the seismic profiles suggest changes of the *P-T* regime and phase composition, with respect to LM's. LM and LLM are assumed to be undistinguishable in terms of bulk geochemical model.

1.2. Deviations from ideality

The present modelling aims to provide a global view of the Fe-periclase compositional trend that stabilises along a chosen geotherm. In order to achieve this, some simplifications were inevitably introduced.

First, the effects of plastic deformation were neglected. In the Fe-periclase/bridgmanite system, the former is supposed to accommodate most of the plastic deformation, which develops through dislocation creeps (Madi et al., 2005). However, much uncertainty still exists about the actual mechanism driving such a phenomenon, its relation to composition and its occurrence throughout the lower mantle (Tommaseo et al., 2006; Cordier et al., 2012; Girard et al., 2016; Reali et al., 2017). Van Orman et al. (2003) observed that the occurrence of dislocations in Al-doped MgO does not seem to extensively affect cation diffusion. This suggests that dislocations modestly influence the octahedral-site force field in periclase, which still preserves its crystal structure and is affected by plastic deformation processes (see the authors quoted above). An approximate estimate of the ratio between energy due to "dislocations" (*i.e.* $\frac{1}{2}\, G_{\text{shear modulus}} \times b^2_{\text{Burgers vector}} \times \rho_{\text{dislocation density}} \times V$) and elastic energy of "hydrostatic deformation" (*i.e.* $P \times (V - V_0)$) gives a value of $\sim 10^{-3}$, using the periclase's elastic constants and dislocation density from Zha et al. (2000) and Miyajima et al. (2014), respectively. Given that the

deformation energy is mostly due to its hydrostatic/elastic contribution we think it reasonable to neglect the dislocation effects.

Another important simplification was to ignore ferric iron. First of all, lower mantle ferric iron is experimentally predicted to preferentially enter bridgmanite (Kurnosov et al. (2017); Frost and Myhill, 2016. In addition, Fe^{3+} is theoretically associated to the appearance of vacancies in non-stoichiometric wüstite and (Mg,Fe)O (Otsuka et al., 2010; Wdowik et al., 2015). Measured iron in Fe-periclase and bridgmanite, both coexisting as inclusions in lower-mantle diamonds (Kaminsky and Lin (2017), reveals that Fe^{3+} un-mixes from periclase lattice, giving rise to clusters of $(Mg_{1+x}Fe^{3+}_{2-x})O_{4-x/2}$. The iron related to Fe-periclase and un-mixed clusters is inferred to be $Fe^{3+}/\Sigma Fe$ 8–12 at%. Given that most iron content values in natural (Mg,Fe)O do not exceed 0.5 FeO (Harte, 2010; Kaminsky, 2012), the vacancy generation effect induced by ferric iron can therefore be assumed negligible in the present modelling.

Finally, the potential effects of metallization of iron were neglected since such a reaction is experimentally observed only in *quasi*-wüstite compositions (Ohta et al., 2014).

2. LOWER MANTLE GEOCHEMICAL FRAME

The pyrolite model provides one of the possible chemical compositions for the Earth's lower mantle. On the basis of phase equilibrium principles and known physical properties of H*P* minerals, the lower mantle turns out to be mainly constituted of $(Mg,Fe)SiO_3$ (bridgmanite), (Mg,Fe)O (Fe-periclase) and $CaSiO_3$ (Ca-perovskite), besides an "undefined H*P* Al-phase" (i.e. Miyajima et al., 2001; Pamato et al., 2014). Such phases occur in proportions that are a function of both geochemical and geophysical models. The former constrains the bulk chemical composition (McDonough and Sun, 1995; Lyubetskay and Korenaga, 2007; Stixrude and Lithgow-Bertelloni, 2007; Merli et al., 2016); the latter accounts for density-pressure-temperature profiles that are consistent with observations (*i.e.*: seismic velocities, density and bulk sound speed; Jackson, 1998; Mattern et al., 2005; de Wit and Trampert, 2015).

Assuming the mantle to be representable by the CMASF system (CaO-MgO-Al_2O_3-SiO_2-FeO), the pyrolitic model's phase composition of the lower mantle consists of ~75–78 wt% $(Mg,Fe)SiO_3$, ~6–10 wt% $CaSiO_3$, ~15 wt% (Mg,Fe)O and ~2 wt% high-pressure Al-rich phase (Ono and Oganov, 2005; Mainprice, 2007; Merli et al., 2016). Given that Ca-perovskite and bridgmanite exhibit similar thermoelastic responses at the reference lower mantle *P*-*T* conditions (Deschamps and Trampert, 2004; Li et al., 2005; Matas et al., 2007), a simplified MgO-SiO_2-FeO system (MSF) was used in the present work.

The conversion from CMASF to MSF consists in replacing Mg + Ca + Al/2 with Mg, and Si + Al/2 with Si. The resulting bulk chemical composition (Table 1) has a Mg/Si molar ratio of 1.20, which is lower than the pyrolitic value (~1.27) but higher than the chondritic one (~1.1). Such a ratio is in agreement with a lower bulk chemical composition slightly enriched in SiO_2 (and FeO) and depleted of MgO, with respect to the pristine pyrolitic model (Deschamps and Trampert, 2004; Matas et al., 2007; Merli et al., 2016). The fractions by weight of Fe-periclase and bridgmanite in the lower mantle were estimated 0.13 and 0.87 (Table 1) respectively, by means of least-square mass balance calculations (Paktunc, 1998; Kobayashi et al., 2005) under the constraint of the LM-LLM bulk chemical composition.

A geotherm (Fig. 1) with a potential temperature of 1920 K at 24 GPa and *T*-vertical-gradient (dT/dz) of ~0.5 K/km (Matas et al., 2007; Ono, 2008; Merli et al., 2016) was assumed for LM (~700–1900 km depth). A geotherm (>80 GPa; >2000 km) with a potential temperature of 2615 K at 96 GPa and a higher *T*-gradient than LM's, *i.e.* $dT/dz \sim 0.85$ K/km (Deschamps and Trampert, 2004; de Koker, 2010; Wicks et al., 2010; de Wit and Trampert, 2015), was instead chosen for LLM (Fig. 1).

3. THERMODYNAMIC APPROACH

The mixing of the MgO and FeO components in the periclase structure was modelled by extending to the H*P*-regime the formalism of Merli et al. (2015) that uses discrete Chebychev polynomial expansions (Barnard et al., 1998) and statistical thermodynamics (Sanchez et al., 1984). A Hartree–Fock/DFT hybrid scheme was adopted to carry out quantum energy calculations (Dovesi et al., 2009) on super-cells.

3.1. Gibbs energy of mixing at high-pressure and high-temperature

A given Fe-periclase composition, expressed by $x = Fe/(Fe + Mg)$ and $(1 - x) = Mg/(Fe + Mg)$, is compatible with many Mg-Fe configurations (Λ), each one corresponding to a specific arrangement of the magnesium and iron atoms. In the frame of the isothermal-isobaric ensemble a system is composed of *N* particles at equilibrium with *P* and *T* (*i.e. NPT*-ensemble). For simplicity, we do not take into account the explicit dependence on *P* and *T* of the thermodynamic potentials, except for the functions $\Xi(P,T,x)$ and $\xi(P,T,x)$, which are related to the *NPT*-ensemble.

$\Xi(P,T,x)$ is defined by Dill et al. (2003) as:

$$\Xi(P,T,x) = \sum_{\Lambda=1,n} \exp\left[-\frac{H(x,\Lambda)}{kT}\right] = \sum_{\Lambda=1,n} \exp\left[-\frac{U(x,\Lambda)_{st} + PV(x,\Lambda)_{st}}{kT}\right] \times Z(x,\Lambda)_{vib} \quad (1)$$

where *n* is the number of all the possible configurations.

The Gibbs function is related to $\Xi(P,T,x)$ in terms of

$$G(x) = -k \times T \times \ln[\Xi(P,T,x)] \quad (2)$$

where: k = Boltzmann constant; st = lattice static contribution; vib = vibration contribution; $Z(x,\Lambda)_{vib}$ = partition function from harmonic approximation for a given Λ–configuration; $H(x,\Lambda)$ = enthalpy for a given Λ–configuration; $U(x,\Lambda)_{st}$ = lattice static energy for a given Λ–configuration. Numerical calculations show that $Z(x,\Lambda)_{vib}$ exhibits, on

Table 1
Lower mantle pyrolite components and mineral compositions in the MSF system obtained by mass balance calculation.

	LM-LLM		
wt%			
SiO_2	49.11		
FeO	10.01		
MgO	40.88		
Bulk mineral proportions			
(Mg,Fe)-*Pvk*[*]	0.87		
Fe-*Pe*	0.13		
r^2	0.17		
Mg/Si	1.20		
	Virtual LM-LLM mineral phases' compositions		
	(Mg,Fe)-*Pvk*[*]	Fe-*Pe*	
wt%			
SiO_2	56.17	–	
FeO	7.20	29.90	
MgO	36.63	70.10	
p.f.u			
Si	1.199	–	
Fe	0.070	0.175	
Mg	0.731	0.825	

LM = lower mantle (24 > P < 80 GPa); LLM = lowermost lower mantle (P > 80 GPa) (Mg,Fe)-*Pvk* = (Mg,Fe)-perovskite (bridgmanite); Fe-*Pe* = ferropericlase.
[*] Approximation for the *reservoir*'s overall chemical composition.

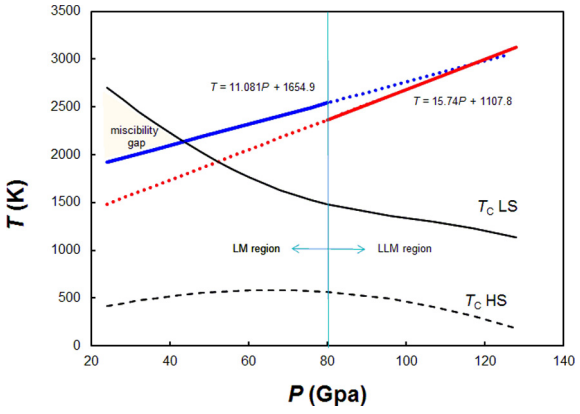

Fig. 1. Geotherms used in the present work, for LM and LLM. LM-geotherm with a potential temperature of 1920 K at 24 GPa and a *T*-gradient (dT/dz) in the range of ~0.5 K/km, is applied to the mantle region of ~24–80 GPa (solid blue line). LLM-geotherm, with a potential temperature of 2615 K at 96 GPa and dT/dz of ~0.85 K/km, is considered in the mantle region of ~80–130 GPa (solid red line). The consolute temperature curves, T_C calculated for LS (solid black line) and HS (dashed black line) state of iron as a function of *P* are also shown. Miscibility gap ($T_C > T_{geotherm}$) occurs between 23 and 42 GPa for LS only.

average, a moderate dependence on the Mg/Fe configuration. Therefore $Z(x,\Lambda)_{vib}$ of Eq. (1) can be replaced with $Z(x)_{vib}$, namely $\langle Z(x,\Lambda)_{vib}\rangle_{\Lambda=1,n}$ (see Section 3.2). From Eq. (2) the Gibbs free energy can be split into two parts: $G(x) = G(x)_0 + G(x)_{vib}$, where $G(x)_0$ collects the static contributions and $G(x)_{vib} = -k \times T \times \ln(Z(x)_{vib})$. Transferring all this to the Gibbs energy of mixing (Ottonello, 1997), we obtain:

$$\Delta G(x)_{mixing} = \Delta G(x)_{0,mixing} + \Delta G(x)_{vib,mixing},$$

where

$$\Delta G(x)_{0,mixing} = -k \times T \times \ln\left\{\sum_{\Lambda=1,n} \exp\left[-\frac{\Delta U(x,\Lambda)_{st,mixing} + P\Delta V(x,\Lambda)_{st,mixing}}{kT}\right]\right\} \quad (3)$$

Δ in Eq. (3) means, for a generic thermodynamic "*A*" quantity of a mixing, the following difference:

$$\Delta A(x)_{mixing} = A(x) - x \times A(\mathrm{FeO}) + (1-x) \times A(\mathrm{MgO}).$$

According to Merli et al.(2015), the sum of Eq. (3) can be approximated, so that

$$\Delta G(x)_{0,mixing} \approx -k \times T \times \ln[\xi(P,T,x)] - \mathrm{R} \times T \times \ln[N(x)_{\mathrm{configurations}}] \quad (4)$$

where R is the gas constant; $N(x)_{\mathrm{configurations}} = \mathrm{N_{Avogadro}}!/\{[x \times \mathrm{N_{Avogadro}}]!\,[(1-x) \times \mathrm{N_{Avogadro}})]!\}$;

$$\xi(P,T,x) = (1/\mathrm{N_{sampled\ configurations}}) \times \sum_{\Lambda=1,\mathrm{sampled\ configurations}} \exp[-(\Delta U(x,\Lambda)_{st,mixing} + P\Delta V(x,\Lambda)_{st,mixing})/kT].$$

The subscript '*sampled configurations*' means that the sum over *all* the possible configurations ($\approx 10^{23}$, for 1 mol) is replaced with a random sampling over an appropriately chosen number of different Fe/Mg arrangements for a given composition, *i.e.* $\mathrm{N_{sampled\ configurations}}$.

3.2. Vibrational contributions to the Gibbs free energy of mixing

Semi-empirical potentials (Lewis and Catlow 1985; Merli et al., 2015), harmonic model and lattice dynamics (GULP code; Gale 1997) were used to calculate $\Delta G(x)_{vib,mixing}$, from random Mg-Fe configurations in 64 cation-sites super-cells over the subsolidus MgO-FeO binary. The range 30–70 GPa and 2000–3500 K was investigated for x-values strewn over the 0–1 interval, sampling up to 10^5 independent configurations. Attention was focussed on how mixing affects $\Delta G(x)_{vib,mixing}$. It was observed that the $G(x,\Lambda)_{vib}$-values oscillate, as a function of the random Λ-configurations, less than 0.1% around $G(x)_{vib}$, *i.e.* their Λ-average, which therefore provides a faithful estimate of the actual vibrational contribution to the Gibbs energy for a given x. $\Delta G(x)_{vib,mixing}$, calculated accordingly, amounts at most to about 2% of the configuration entropy contribution. Given that in the present case the harmonic $\Delta G(x)_{vib,mixing}$ contribution is very modest, then the anharmonic one is expected to be negligible. Altogether, P seems to make the vibrational contribution to the Gibbs energy of mixing of marginal importance for (Mg,Fe)O. Neglecting $\Delta G(x)_{vib,mixing}$ at high pressure is in contrast to what observed at room conditions (Merli et al., 2015), where a small, but significant vibrational contribution (10–15%) participates in the Gibbs energy of mixing.

3.3. Cluster expansion

$\Delta U(x,\Lambda)_{st,mixing} + P\Delta V(x,\Lambda)_{st,mixing}$ was computationally modelled exploiting the formalism that relies upon the cluster-expansion (Yuge 2010) and discrete Chebyschev polynomials (Sanchez et al. 1984; Merli et al., 2015). Such an approach leads to the following expression for $\Delta U(x,\Lambda)_{st,mixing} + P\Delta V(x,\Lambda)_{st,mixing}$ of a given Λ-configuration:

$$\begin{aligned}\Delta U(x,\Lambda)_{st,mixing} + P\Delta V(x,\Lambda)_{st,mixing} \\ \approx \Delta H(P)_0 + \Delta H(P)_1 \times x + x \times (1-x) \times [A(P)_0 \\ + A(P)_{\mathrm{Fe}} \times x] + \sum_{\mathrm{j}=1,number\ of\ clusters} A(P)_{\mathrm{Fe-Mg,j}} \\ \times n(x,\Lambda)_{\mathrm{Fe-Mg,j}} \end{aligned} \quad (5)$$

This equation accounts for a Vegard-like residue; $A(P)_0$ and $A(P)_{\mathrm{Fe}}$ contribute to a composition dependent parabolic term; $A(P)_{\mathrm{Fe\text{-}Mg,j}}$s weigh the number of Fe-Mg couples, *i.e.* $n(x,\Lambda)_{\mathrm{Fe\text{-}Mg,j}}$, whose atoms are d_{j} apart from one another, and constitute the jth-cluster. $\Delta H(P)_{\mathrm{j}}$ and $A(P)_{\mathrm{k}}$ are functions of the pressure and were modelled by polynomials like

$$\omega_{\mathrm{j}}^{(0)} + \omega_{\mathrm{j}}^{(1)} \times P^{\nu(\mathrm{j})} + \omega_{\mathrm{j}}^{(2)} \times P^{\chi(\mathrm{j})} + \ldots \quad (6)$$

The χ, ν,... exponents for each j-coefficient were determined by a trial-and-error approach, whereas the $\omega_{\mathrm{j}}^{(0,1,2,\ldots)}$-coefficients were obtained by fitting the expression given by Eq. (5) to the values calculated by quantum-mechanics. Preliminary tests indicated that parabolic expansions are appropriate for Eq. (6); adding higher order terms does not enhance the quality of the results. Eventually, using Eqs. (5) and (6), $\xi(P,T,x)$ of Eq. (4) was calculated by sampling $\sim 10^6$–10^8 Λ-configurations (Merli et al., 2015), which guarantee negligible oscillations of the resulting $\Delta G(x)_{0,mixing}$.

3.4. Ab-initio calculations

Static enthalpy calculations and structure relaxation were carried out at a given 0 K pressure by the HF/DFT-CRYSTAL14 program (Dovesi et al. 2009), which implements "A*b-initio* Linear-Combination-of-Atomic-Orbitals" in the case of periodic systems. Pressure was corrected for zero point and thermal contribution following Merli et al. (2016). A Hamiltonian based on the WC1LYP functional (Scanavino et al. 2012; Scanavino and Prencipe 2013) was used in the present work, along with the flexible HF-DFT hybrid scheme earlier discussed and adopted for (Mg,Fe)O at room pressure by Merli et al. (2015). It relies upon mixing HF and DFT exchange energy contributions, in terms of a Hartree-Fock fraction ($\mathfrak{I}_x$) given by $\mathfrak{I}_x = (1-x) \times \mathfrak{I}_{\mathrm{MgO}} + x \times \mathfrak{I}_{\mathrm{FeO}} + x \times (1-x) \times \mathfrak{I}_{\mathrm{MgO}} \times \mathfrak{I}_{\mathrm{FeO}}$ (hybridization, tuning of functional and delocalization error: Alfredsson et al., 2004; Autschbach and Srebro, 2014). For the end-members the following hybridization rates were used: $\mathfrak{I}_{\mathrm{FeO}} = 0.16$ (HS; calibration on the band gap) and 0.24 (LS; calibration on the HS to LS transition at 40 GPa, for $x = 0.2$); $\mathfrak{I}_{\mathrm{MgO}} = 0.2$ (calibration on the band gap). Such an approach has proven effective to yield mixing energies that are weakly sensitive to change of the end members' hybridization rate. Tests performed at room pressure show that shifts even by 30–35% of $\mathfrak{I}_{\mathrm{MgO\text{-}FeO}}$ lead to mixing enthalpy average changes within 5–10%. The following values were used for the tolerance governing the accuracy of the integrals of the self-consistent-field-cycles: 10^{-6} for coulomb overlap, 10^{-6} for coulomb penetration, 10^{-6} for exchange overlap, 10^{-6} for exchange pseudo-overlap in direct space, 10^{-12} for exchange pseudo-overlap in reciprocal space and 10^{-9} a.u. threshold for SCF-cycles' convergence. The Mg basis set from Causà et al. (1986) was extended by the addition of diffuse *sp* and *d* shells (85-11G* contraction). The O basis set of Ottonello et al. (2010) was used, modified by the introduction of a *d* shell (84-11G* contraction) according to Belmonte et al. (2014). The Fe basis set is from Valerio et al. (1995). The ability to reproduce physical observables of MgO and FeO using the present computing set-up is discussed by Merli et al. (2015, 2016).

The static contributions to the Gibbs free energy of the substance at 4–6 independent Λ–configurations were calculated using super-cells of 16 cation sites to obtain multiplicity-weighted average $\Delta U + P\Delta V$'s for each LS-composition of $x \sim 0.125$–0.25–0.375–0.5–0.625–0.75–0.875, at 24–40–70–90–110–128 GPa. The HS-state was treated alike, but restricting calculations to $x \sim 0.125$–0.375–0.50–0.75–0.875, at 24–60–80–110 GPa. The approach of Merli et al. (2015) was followed to model a HS-paramagnet, by resorting to disordered up and down spin configurations such as yield a total residual spin of zero.

The average $(\Delta U + P\Delta V)$-values were then fitted by polynomials in x to get by interpolation additional

($\Delta U + P\Delta V$)-values, strewn over the 0–1 x-range, at every explored P. Eqs. (5), (6) were eventually fitted to the obtained set, using average $n(x)_{\text{Fe-Mg,j}} = \langle n(x,\Lambda)_{\text{Fe-Mg,j}} \rangle_\Lambda$ calculated over 10^5-configurations for each given x. A cut-off of 10 Å was chosen after tests to fix up the size of the clusters of expansion (5). By means of the $\Delta H(P)_k$ and $A(P)_j$ coefficients, the static term $\Delta U(x,\Lambda)_{st,mixing} + P\Delta V(x,\Lambda)_{st,mixing}$ was calculated for super-cells of 1024 Fe/Mg-atoms, and thereby $\Delta G(x)_{0,mixing}$ was determined according to Eq. (4).

Given the fact that the vibrational contributions are negligible, we introduce the following approximation: $\Delta G(x)_{mixing} \approx \Delta G(x)_{0,mixing}$ and hereafter use $\Delta G(P,T,x)_{mixing}$ to indicate the bulk Gibbs free energy of mixing at P-T conditions and x FeO, calculated accordingly.

3.5. Reaction model

Once $\Delta G(P,T,x)_{mixing}$ is determined, it can be used to investigate the (Mg,Fe)O mixture at subsolidus and its interactions with the *reservoir* through irreversible disequilibrium reactions, implying an exchange of matter between *reservoir* and Fe-periclase.

We start from the basic reaction:

$$(Mg_{1-x0}Fe_{x0})O \Longleftrightarrow y1(Mg_{1-x1}Fe_{x1})O + y2(Mg_{1-x2}Fe_{x2})O \quad (7)$$

where xi is the ith FeO fraction, and yi is the ith phase fraction related to the Fe-periclase having xi FeO. To fulfil the mass conservation principle, $y1$ and $y2$ of Eq. (7) result in (see Appendix A, for derivation):

$$y1 = \frac{(x0 - x2)}{(x1 - x2)} \quad (8.a)$$

$$y2 = 1 - y1. \quad (8.b)$$

Reaction (7) is dealt with from two points of view: one related to a *closed system*, and another to an *open system*.

A *closed system* is modelled in terms of a given (Mg,Fe)O-phase that can un-mix into two more stable compositions, according to the MgO-FeO binodal/spinodal curves (Ottonello 1997; for application to the MgO-FeO system at room pressure see Merli et al. 2015). Un-mixing is intimately linked to the Gibbs energy minimization under the constraint of equality of chemical potentials. The consolute temperature, T_C, defines the upward limit of a miscibility gap in a T-X Schreinemaker projection, *i.e.* the temperature above which un-mixing processes do not occur, for a given P, and solid mixings are stable.

Alternatively, an *open system* is modelled, treating Eq. (7) in terms of forward and backward reactions, in which the left- and right-hand side members act both as reagents and products and equilibrium is achieved when forward and backward rates are equal to one another. Eq. (7) is a simplification of the possible more complex natural reactions involving a larger number of reactants and products. $x0$ is a 'reference pivot-composition', which is supposed to exist at any P-T point of both LM and LLM geotherms, along with the compositions given by $x1$ and $x2$ (Appendix B). The $x0$-value can be taken over the interval 0.15–0.20 FeO, since: (i) this range includes the average FeO content of Fe-periclase inferred by the geochemical model (Table 1); (ii) it accounts for the most frequent Fe-periclase's compositions observed both in natural findings from lower mantle samples (Harte, 2010; Kaminsky, 2012) and in Fe/Mg partitioning experiments (Auzende et al., 2008; Nakajima et al., 2012; Prescher et al., 2014). In this model, the (Mg,Fe)O-system achieves P-T-X equilibrium with a thermodynamic matter *reservoir*, which behaves as an ideal Fe/Mg exchanger (see Appendixes B and C for a description of the disequilibrium-to-equilibrium process, involving Fe-periclase and *reservoir*). Such a matter *reservoir* is the portion of lower mantle other than Fe-periclase and can be likened, in terms of *bare* MSF-composition, to a "virtual" (Mg,Fe)-perovskite (Table 1).

The phase proportions of the solid mixings that correspond to the $x0$-, $x1$- and $x2$-compositions are addressed here by means of λ0, λ1 and λ2, respectively. Note that

$$\lambda 0 + \lambda 1 + \lambda 2 = 1. \quad (8.c)$$

The equilibrium constant of the reaction (7) is

$$K(P,T,x0,x1,x2) = \exp\left[-\frac{(\Delta G(P,T,x0)_{mixing} - y1 \times \Delta G(P,T,x1)_{mixing} - y2 \times \Delta G(p,T,x2)_{mixing})}{RT}\right] \approx \frac{\lambda 0}{(\lambda^{y1} \times \lambda^{y2})}, \quad (9)$$

where the activity coefficient is approximated by unity.

For each {$x0$-$x1$-$x2$}-set we seek for the {λ0, λ1, λ2}-set that minimises the function

$$\Delta G(P,T,x0,x1,x2)_{\text{Total}mixing} = \lambda 0 \times \Delta G(P,T,x0)_{mixing} + \lambda 1 \times \Delta G(P,T,x1)_{mixing} + \lambda 2 \times \Delta G(P,T,x2)_{mixing}, \quad (10)$$

under the constraints given by Eqs. (8.a-b-c and 9).

Such an approach implies that:

(i) an exchange of FeO/MgO between (Mg,Fe)O-system and lower mantle *reservoir* takes place *via* λ0-λ1-λ2 under the sole constraint that the global bulk (FeO + MgO) content must be preserved, so that Fe-periclase gives Δx-moles of FeO(MgO) to the *reservoir* and takes as many moles of MgO(FeO) from it;

(ii) the point above requires that the incorporation of FeO/MgO into the *reservoir* causes variations of its Gibbs energy that are assumed of the same order of magnitude of the oscillations occurring because of the many reactions in the lower mantle (Appendix C). Such an assumption is equivalent to taking Fe-periclase as the pivot-exchanger for iron/magnesium in the deep interior of the Earth. This is consistent with that the Fe/Mg partitioning coefficient between bridgmanite (the other main mineral competitor for incorporation of Fe) and Fe-periclase is observed to be significantly smaller than 1, *i.e.* (Mg,Fe)O is the main host of iron.

The λj-values, determined according to Eqs. (9) and (10), depend on $x0$, $x1$, $x2$, P and T, so that λj($x0$, $x1$,

$x2$), dropping for brevity P and T. Given that we are interested in average values, mean phase proportions, $\langle \lambda j \rangle$, were obtained by a numerical integration over the allowed $x0$, $x1$ and $x2$ ranges (note that $x2 < x0 < x1$, due to that $0 < y1 < 1$), that is:

$$< \lambda j >= C \int_{x0-inf}^{x0-sup} dx0 \int_{x0}^{1} dx1 \int_{0}^{x0} \lambda j\,(x0, x1, x2)\, dx2 \qquad (11)$$

where C is a normalization factor, $x0\text{-}sup = 0.20$ and $x0\text{-}inf = 0.15$.

$\langle x0 \rangle$, $\langle x1 \rangle$ and $\langle x2 \rangle$ are calculated as $\langle \lambda j \times xj \rangle / \langle \lambda j \rangle$. This way, $\langle \lambda 0,1,2 \rangle$ and $\langle x1,2 \rangle$ depend on P-T only, and show how the (Mg,Fe)O-system changes along a pressure-temperature path in terms of Mg-Fe-solid mixings. Note that Eq. (7) and integration $x0$-interval imply that $\langle x0 \rangle$ is equal to 0.175.

In the ensuing discussions, the notations xj (jth-phase's composition) and λj (jth-phase proportion) will be used in place of $\langle xj \rangle$ and $\langle \lambda j \rangle$ from Eq. (11), for simplicity.

3.6. Spin state and excess Gibbs energy of mixing

LS-HS mixed states, which affect the physical properties of the (Mg,Fe)O-phases, are often accounted for in a solid mixing by a linear combination of the pure LS and HS systems (Lyubutin et al., 2009; Wentzcovitch et al. 2009; Muir and Brodholt, 2015; Vilella et al., 2015). It is straightforward to prove that in a HS-LS-(FeO-MgO) system ($x^{\text{LS-HS}}$-x^{LS}-x^{HS} being x- FeO in mixed HS-LS state, pure LS or HS state, respectively) the exact mixing energy is expressible as

$$\begin{aligned}\Delta G(P,T,x^{\text{LH-HS}})_{mixing} &= \eta \times \Delta G(P,T,x^{\text{LS}})_{mixing} \\ &+ (1-\eta) \times \Delta G(P,T,x^{\text{HS}})_{mixing} \\ &+ \{G(P,T,x^{\text{LS-HS}}) - \eta \\ &\times G(P,T,x^{\text{LS}}) - (1-\eta) \\ &\times G(P,T,x^{\text{HS}})\}, \end{aligned} \qquad (12)$$

where $\eta = 1/(1 + \exp((G^{\text{LS}}\text{-}G^{\text{HS}})/x\text{R}T))$. In principle, it is possible to calculate the quantity $G(x^{\text{LS-HS}},P,T)$, but in practice it is difficult, because of the exceedingly large super-cell size required in order to achieve statistical representativeness and faithfulness, and of the many configurations to explore. However, if we assume that the third term of the right-hand side member of the Eq. (12) is negligible, then the equilibrium constant, *i.e.* Eq. (9), becomes:

$$\begin{aligned} K(P,T,x0,x1,x2) &= \exp[-\eta \times \Delta G(P,T,x0,x1,x2)^{\text{LS}}_{mixing}/\text{R}T] \\ &\times exp[-(1-\eta) \\ &\times \Delta G(P,T,x0,x1,x2)^{\text{HS}}_{mixing}/\text{R}T] \\ &\approx [K(P,T,x0,x1,x2)^{\text{LS}}]^{\eta} \\ &\times [K(P,T,x0,x1,x2)^{\text{HS}}]^{(1-\eta)} \\ &= \left\{\left[\frac{\lambda 0}{\lambda 1^{y1} \times \lambda 2^{y2}}\right]^{\text{LS}}\right\}^{\eta} \\ &\times \left\{\left[\frac{\lambda 0}{\lambda 1^{y1} \times \lambda 2^{y2}}\right]^{\text{HS}}\right\}^{(1-\eta)} \end{aligned} \qquad (13)$$

where two sets of "virtual" phase proportions of the $x0$-1-2-phases are defined, *i.e.* $[\lambda 0, \lambda 1, \lambda 2]^{\text{LS}}$ and $[\lambda 0, \lambda 1, \lambda 2]^{\text{HS}}$. LS and HS can be treated as decoupled states, with respect to the constraint given by Eq. (13). Although such approximation provides an "extreme" depiction, as only pure spin states are involved, it gives a general view of how far either spin state affects the reactivity of the (Mg,Fe)O-system and guarantees the required precision to treat small and complex quantities such as mixing energy.

Using the cluster expansion technique (see Section 3.3), we generated $\Delta G(P,T,x)_{mixing}$ data for either iron state and interpolated them by Redlich–Kister-type expressions (Stølen and Grande 2004), which model the mixing Gibbs energy as

$$\begin{aligned}\Delta G(P,T,x)_{mixing} &= x \times (1-x) \times h(P,T,x) + \text{R} \times T \times [x \\ &\times \ln(x) + (1-x) \times \ln(1-x)],\end{aligned}$$

where the first term of the right-hand side member gives the excess enthalpy, and

$$h(P,T,x) = \sum_{l=0,L;m=0,M;n=0,N} p_{lmn} \times P^l \times T^m \times x^n.$$

The p_{lmn}-parameters of the expansion above for LS and HS (interval: $x = 0$–1, $T = 1900$–4000 K, $P = 24$–140 GPa) are reported in Table 2.

4. RESULTS

4.1. Un-mixing processes in closed (Mg,Fe)O-system

Our calculations predict that at lower mantle P-T conditions, HS never gives rise to un-mixing reactions in the MgO-FeO system at subsolidus, as $T_{\text{C}} < T_{\text{geotherms}}$ (Fig. 1). LS, too, yields T_{C} values that are smaller than the temperatures of both LM and LLM geotherms (Fig. 1), but for the shallowest portions of the lower mantle (~23–42 GPa). Pure LS gives un-mixings between 0.24 and 0.84 FeO (Fig. 2), at the base of the immiscibility region ($T_{\text{C}} = 1920$ K, $P = 24$ GPa), and between 0.50 and 0.65 FeO, at its top ($T_{\text{C}} = 2174$ K, $P = 42$ GPa). Given that for reference Fe-periclase composition, HS on average prevails up to ~40 GPa (Fei et al., 2007; Lin et al., 2007) and stabilizes solid mixings (Fig. 1), it is unlikely that the un-mixed products due to LS can provide an important contribution in nature below ~40 GPa.

It is important to note that almost all the experiments agree to exclude that Fe-periclase un-mixes at lower mantle conditions. Lin et al. (2003) and Ohta et al. (2014), who explored the compositional range from 0.61 to 0.95 FeO, did not observe any disproportionation, except for *quasi*-wüstite compositions (140 GPa–2580 K). Conversely, Dubrovinsky et al. (2000, 2001) report un-mixing of (Mg,Fe)O, with x up to about 0.5 FeO, into Mg-rich and Fe-rich periclase like phases, but at conditions far from lower mantle's (86 GPa and 1000 K). However, the relevant variety of Fe-periclase compositions observed in the lower mantle diamond inclusions (Kaminsky, 2012 and reference therein) and in the samples from Fe/Mg bridgmanite/Fe-periclase partitioning experiments (Auzende et al., 2008; Nakajima et al., 2012; Prescher et al., 2014) has to be explained.

Table 2
h-function coefficients, p_{lmn}. $h(P,T,x) = \Sigma_{l=0,L;m=0,M;n=0,N}\ p_{lmn}\ P^l\ T^m\ x^n$, in kJ/mol. P in GPa, T in K.

LS	l	m	n	HS	l	m	n
2.6464E+01	0	0	0	7.9787E+00	0	0	0
1.2452E−03	0	1	0	−5.3230E−05	0	1	0
−4.1031E−01	1	0	0	1.6842E−01	1	0	0
3.7372E−05	1	1	0	1.8179E−05	1	1	0
−6.2807E−05	2	0	0	−1.7149E−03	2	0	0
−6.4309E−07	0	2	0	−2.3683E−07	0	2	0
7.4246E−11	0	3	0	3.0516E−11	0	3	0
−1.5820E−09	1	2	0	−5.8064E−10	1	2	0
5.6086E+01	0	0	1	−2.6739E+00	0	0	1
1.2233E−02	0	1	1	8.7180E−03	0	1	1
−1.2437E+00	1	0	1	−9.6506E−01	1	0	1
7.3130E−03	2	0	1	6.5342E−03	2	0	1
−9.1533E−08	0	2	1	−6.1504E−07	0	2	1
−3.5835E−04	1	1	1	−1.4678E−04	1	1	1
3.6238E+00	0	0	2	1.0566E−11	2	2	1
1.5120E+00	1	0	2	1.6068E+01	0	0	2
−3.9686E−02	0	1	2	9.7615E−01	1	0	2
−9.3201E−03	2	0	2	−1.5066E−02	0	1	2
4.7498E−08	0	2	2	−6.4031E−03	2	0	2
1.3609E−03	1	1	2	1.0064E−06	0	2	2
−6.7874E+01	0	0	3	4.6602E−04	1	1	2
3.4580E−01	1	0	3	−1.5936E+01	0	0	3
3.6984E−02	0	1	3	−1.3987E−01	1	0	3
−1.8915E−03	1	1	3	6.7423E−03	0	1	3
7.3964E−04	1	1	4	−7.0532E−04	1	1	3
6.7373E−07	2	1	4	2.8506E−07	2	1	3
				−1.2780E−09	1	2	3
				3.5260E−04	1	1	4
				−5.5021E−15	2	3	4

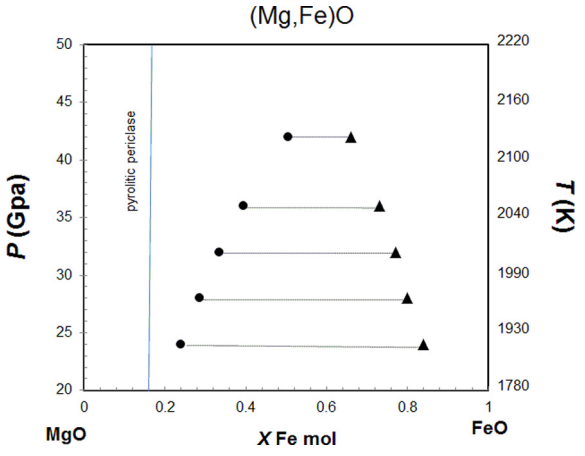

Fig. 2. Predicted miscibility gap for LS in the MgO–FeO binary system, as a function of pressure and temperature. P-T values from the geotherms here used. The pyrolitic Fe-periclase reference $x0$-composition ($x = 0.175$ FeO) is also reported.

4.2. Extension to the MgO - FeO - SiO2 system

The wide range of Fe-periclase compositions (the statistically most relevant interval is ~0.3–0.5 FeO) observed both in natural findings and in HP-HT syntheses suggests that the (Mg,Fe)O-system can be modelled by reactions according to Eq. (7), which imply forward-backward transformations and may include exchange of matter with the surroundings.

Fig. 3a and b shows xj and λj as function of P, along the lower mantle geotherms, for LS and HS. All the compositions exhibit slight changes (not graphically appreciable) in the case of HS over the explored P range (Fig. 3a), whereas a significant enrichment in Fe occurs in the x1-phase for LS. The phase proportions of the x0-, x1- and x2-phases (Fig. 3b) remarkably vary along the geotherms in the case of LS, only.

$\langle K(P,T)\rangle$ as function of P (Fig. 4a), namely the average equilibrium constant obtained by an integration over the allowed $x0$-$x1$-$x2$ ranges of Eq. (7), provides a partial explanation for the insensitivity to P-T of the HS's λ-values (Fig. 3b). In fact, LS exhibits a significantly steeper trend than HS, along the LM-LLM-paths ($\partial\langle K(P,T)\rangle/\partial P \approx 9\ 10^{-4}$ and $2\ 10^{-4}$ GPa^{-1}, for LS and HS, respectively), suggesting that different mixing behaviours take place as a function of the spin state. The average equilibrium constant for HS is, in practice, *quasi*-invariant over the LM and LLM mantle regions (Fig. 4a). In addition, the LS-HS excess enthalpy functions (ΔH_{excess}), at

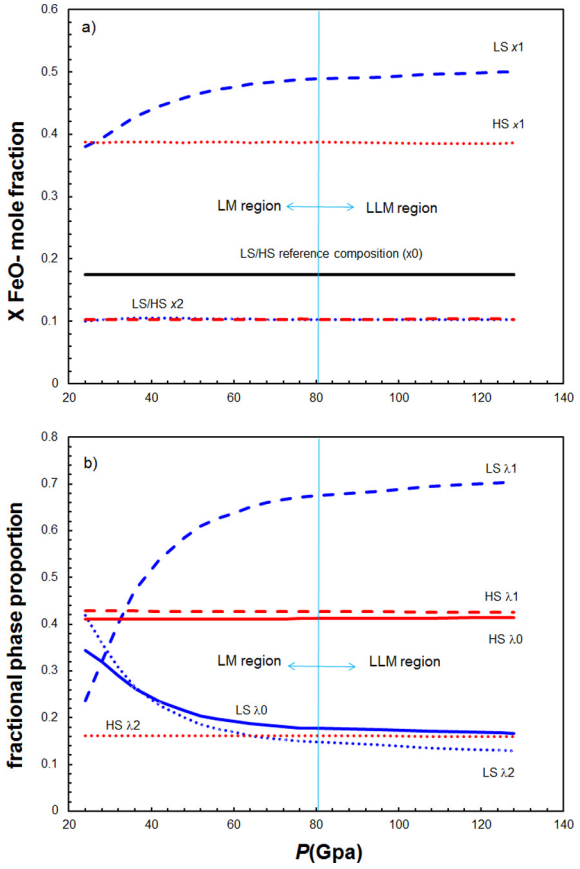

Fig. 3. LS: blue; HS: red. (a) Compositions of the x0-, x1- and x2-phases (solid, dashed and dotted lines, respectively) in terms of FeO fractions; (b) phase proportions λ0, λ1 and λ2 (solid, dashed and dotted lines, respectively) of x0-, x1- and x2-mixings, respectively. (For interpretation of the references to colour in this figure legend, the reader is referred to the web version of this article.)

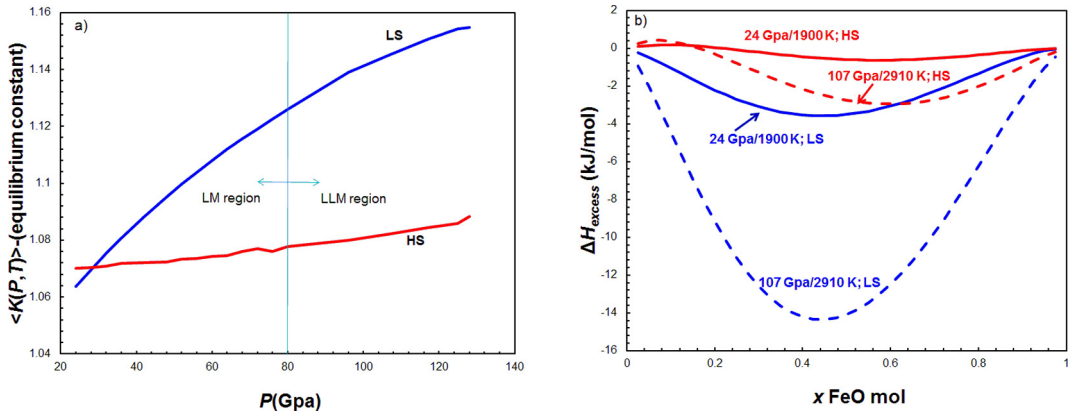

Fig. 4. LS: blue; HS: red. (a) The average equilibrium constant, $\langle K(P,T)\rangle$, is plotted according to Eqs. (7)–(11) in the text, along the LM-LLM-paths; (b) static excess enthalpy (ΔH_{excess}) determined at 24/1900-107/2910 GPa/K, as an example of the LM and LLM mantle regions, respectively. (For interpretation of the references to colour in this figure legend, the reader is referred to the web version of this article.)

24/1900-107/2910 GPa/K, show relevant differences (Fig. 4b). LS has larger absolute ΔH_{excess} and $d\Delta H_{mixing}/dx$ values than HS; this underlies that the LS (Mg,Fe)O-system is more sensitive to *P-T* in terms of equilibrium constant than HS. LS and HS exhibit excess enthalpy curves similar in shape at 24 GPa, but they remarkably change at 107 GPa, in such a way that the two spin states yield opposite trends (Fig. 4b).

5. DISCUSSION

On the basis of these results, LS can be consider the main booster of phase changes in the (Mg,Fe)O-system over most of the LM and LLM regions. Therefore, we focus on the results of the LS-state only.

The $x2$-phase (FeO $\sim$ 0.10, at 24 GPa) mimics the $x0$-phase (FeO $\sim$ 0.175 as inferred by the bulk geochemical model), showing slight changes in composition along the geotherms (Fig. 3a). This implies that both $x2 = Mg_{90}Fe_{10}$-phase and, obviously, $x0 = Mg_{82}Fe_{18}$-reference-phase are products in the (Mg,Fe)O-system, which occur at any *P-T* of the lower mantle regions.

Conversely, the $x1$-phase [$(Mg_{0.61}Fe_{0.39})O$ at 24 GPa] remarkably changes in composition with respect to both $x0$ and $x2$, increasing over the entire LM region (up to ~80 GPa) its Fe-content up to 0.49 (Fig. 3a). This leads to an enrichment of 0.1 FeO from 24 to 80 GPa; at higher pressure (LLM region), the $x1$-phase stabilises at ~0.5 FeO content (Fig. 3a).

At 24 GPa, the $x0$-$x1$-$x2$-phases occur in proportions of $\lambda 0 \approx 0.34$, $\lambda 1 \approx 0.23$ and $\lambda 2 \approx 0.43$ (Fig. 3b), respectively. The iron rich $x1$-phase is the least abundant in the uppermost part of the lower mantle, but rapidly increases exceeding $x0$- and $x2$-phases at some 30 GPa, along the LM geotherm. At 80 GPa (~2000 km depth), the $x1$-phase, $(Fe_{0.5}Mg_{0.5})O$, reaches the proportion of $\sim$ 0.67. Deeper, in the region of the LLM geotherm (80–130 GPa), the iron rich $x1$-phase keeps on being the most abundant reaction product in the (Mg,Fe)O-system (Fig. 3b). This suggests that the modelled possible products of the (Mg,Fe)O-system in the LLM region are highly stable, invariant in composition and proportion.

Moreover, we observe that the $x1$-phase is the major exchanger with the *reservoir*; this is consistent with the fact that the $x1$-composition is the most distant among $x0$-1-2-phases' from *reservoir*'s, thus suggesting the occurrence of elemental concentration gradients that promote flow of matter. In turn, the $x2$-phase's comparatively low amount might be related to a high activation energy to achieve the critical size of nucleation that triggers then crystal growth.

As expected, the density (ρ) of the $x0$-$x1$-$x2$-phases progressively increases as function of *P* (Fig. 5). At 24 GPa, the most dense $x1$-phase [$(Fe_{0.39}Mg_{0.61})O$; $\rho_{x1} = 5.3$ g/cm^3] is also the least abundant (Fig. 3b), whereas the $x0$- and $x2$-phases, which share almost equal density values (4.6 and 4.3 g/cm^3, respectively), together account for $\sim$ 0.80 phase proportion in the (Mg,Fe)O-system (Fig. 3b; Fig. 5). Consequently, the average density of the (Mg,Fe)O-system in the shallow part of the lower mantle (~700 km) is controlled by iron poor phases (~4.5 g/cm^3). It is worth noting that the density of the $x1$-phase increases linearly in the LLM region, even if the $x1$-phase ceases to incorporate additional iron from the *reservoir* at about 80–90 GPa. This implies that below ~2000 km depth, the bulk density of the (Mg,Fe)O-system (6.5 g/cm^3, using the LLM geotherm), primarily depends on the pure physical properties of the involved phases, which are invariant in composition and phase fractions from $\sim$ 90 GPa to the core-mantle boundary. Moreover, if the (Mg,Fe)O-system is considered as constituted by $x1$ and $(x0 + x2)$ only, then they yield a net change in terms of differential density, *i.e.* $\Delta\rho = [\rho_{x1} - (\rho_{x0} + \rho_{x2}) \times 0.5]$, from 0.8, at 24 GPa, to 1.4, at 130 GPa. This corresponds altogether to a mean $\Delta\rho$-increase of approximately 10%, in keeping with the results of Rost et al. (2005) and McNamara et al. (2010).

On the whole, the lower mantle (Mg,Fe)O-system with the pyrolitic reference composition 0.175 FeO (Table 1)

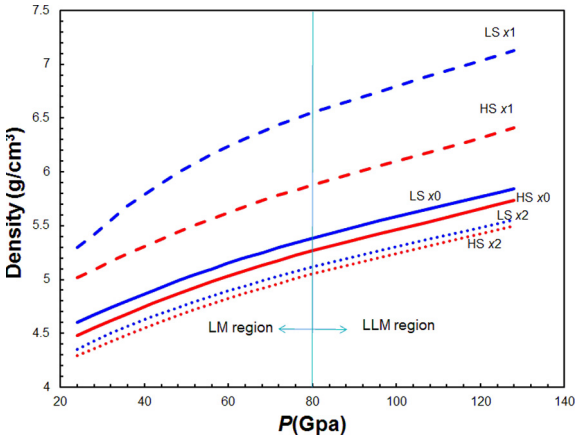

Fig. 5. Density (g cm^{-3}) of the $x0$-, $x1$- and $x2$-phases (solid, dashed and dotted lines, respectively) in the case of LS (blue) and HS (red). (For interpretation of the references to colour in this figure legend, the reader is referred to the web version of this article.)

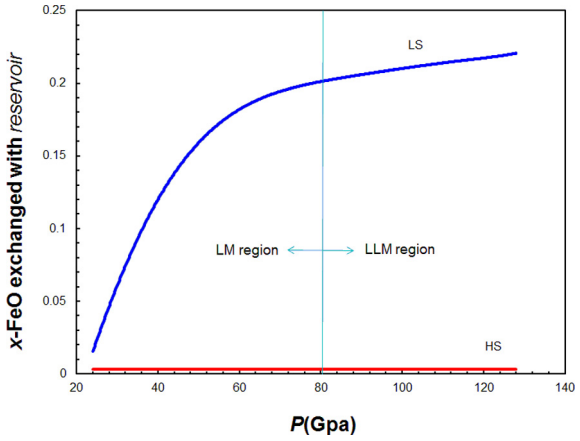

Fig. 6. LS: blue; HS: red. FeO-fraction excess with respect to the reference $x0$-composition due to exchange between Fe-periclase and *reservoir*, in open (Mg,Fe)O-system. (For interpretation of the references to colour in this figure legend, the reader is referred to the web version of this article.)

tends to acquire iron from the *reservoir* upon increasing pressure, for a maximum *total* enrichment of ~0.22 FeO and by effect of LS only (Fig. 6).

Following the suggestion of iron-rich starting material used in a few Fe/Mg periclase/bridgamite partitioning experiments (Nakajima et al., 2012), a fictitious 'not-pyrolitic' lower mantle (Fe,Mg)O-system with a reference composition $x0 = 0.3$ FeO was also modelled, in order to test the sensitivity of Eq. (7) to $x0$ in the case of LS. This system results in a weaker exchanger with the *reservoir* (<0.09 Fe at ~130 GPa) in comparison with the pyrolitic model, and the compositions of the resulting phases scarcely change along both the LM and LLM *P-T* paths. The Fe-rich phase occurs with ~0.55 FeO at 24 GPa, ~0.51 FeO at 48 GPa and then slightly increases its iron content to ~0.52 FeO at ~130 GPa. These data reflect an iron-saturation effect in the (Mg,Fe)O-system, owing to an unduly large $x0$-value for the reference composition with respect to the pyrolitic model (Table 1, Fig. 3).

For the sake of completeness, it is worth pointing out that a simultaneous occurrence of LS and HS depicts the most likely Earth's lower mantle iron state (Lin et al., 2013). We approximately estimated the LS-HS effects by linearly combining the results from one spin state with those of the other using the η-weighting function (see Eq. (13)). In so doing and leaving aside any claim of precision, the composition of the $x1$-mixed-states-phase achieves the same "saturation" value as for pure LS of 0.5 FeO upon *P*, at about 100 GPa. The general trends of the phases' compositions and phase proportions in mixed spin states as a function of the geotherms are preserved with respect to pure LS's, although they are shifted by ~20 GPa to higher *P*-values. Despite the level of approximation we have to accept in view of the complexity of the reactions occurring in the lower mantle, altogether our results corroborate that $(Fe_{0.5}Mg_{0.5})O$-phase is expected to be the likeliest Fe-rich periclase composition in the LLM region (from 80–100 GPa), independently of the $x0$-reference composition. This is in agreement with the results of multicomponent experiments that, using as starting material the San-Carlos olivine (0.3 FeO), yield Fe-periclase whose highest iron content is 0.487 FeO (Nakajima et al., 2012). We are aware that a direct comparison between theoretical and experimental results has to be taken with due care. In fact, H*P*-H*T* experimental set-up, reaction kinetics and compositional constraints significantly affect the results, causing deviations from expectations (*i.e.* high temperature effects on transformations, occurrence of gradients, metastability, complex REDOX-reactions).

5.1. Fe/Mg partitioning between reservoir and Fe-periclase

Using the *reservoir*'s composition (likened to a "virtual" bridgmanite's; Table 1) and the predicted (Mg,Fe)O-phases, the bulk Fe/Mg partitioning between *reservoir* and Fe-periclase $[Kd = (Fe/Mg)^{reservoir}/(Fe/Mg)^{Fe\text{-}periclase}]$ was calculated. In this view, Kd may be considered as an approximate estimate of the actual partitioning between bridgmanite and Fe-periclase, yet taking into account that we are neglecting the *reservoir*'s energetics and therefore we assume that the Fe/Mg exchange/equilibration is driven by the (Mg,Fe)O-system only, as already stated. Kd is determined weighting the Fe-periclase $x0$-$x1$-$x2$-phases by their proportions.

In the LM region, when the LS state drives the degree of iron reactivity, a continuous decrease of Kd from 0.64 to 0.19 can be observed. At higher pressures, in the LLM region, where the (Mg,Fe)O-system's phases do not significantly change, neither in composition nor in proportion, the bulk Fe/Mg-Kd is almost constant ($Kd = 0.18$–0.16 between ~80 and 130 GPa). If the Fe/Mg partitioning between *reservoir* and Fe-periclase is calculated treating each xj-phase as independent of the others, then Kd-intervals of 0.5–0.3, 0.18–0.06 and 1–0.5, for $x0$, $x1$ and $x2$, respectively, are obtained. This means that the (Mg,Fe)O-phases exhibit diverse attitudes to iron hosting.

In addition, if a mixed spin state of ferrous iron was taken into account, the Kd-values would increase because of the HS contribution. However, using the compositions and phase proportions obtained from HS-LS linear combination, the Fe-Mg partitioning trend does not change with respect to LS's, with Kd-values as large as 0.19–0.16 in LLM region.

Our results of Fe/Mg partitioning between *reservoir* and Fe-periclase agree with experimental and theoretical studies on pyrolitic and Al-free systems, which give Kd, for bridgmanite/Fe-periclase, ranging from 0.6 to 0.06 (*i.e.* Deschamps and Trampert, 2004; Kobayashi et al., 2005; Auzende et al., 2008; Sakai et al., 2009; Nakajima et al., 2012; Prescher et al., 2014; Muir and Brodholt, 2015). In particular, H*P*-H*T* experiments carried out between 30–130 GPa and 1760–2500 K (Prescher et al. 2014; Sinmyo et al., 2008; Sinmyo and Hirose, 2013; Narygina et al., 2011) yield Kd-estimates showing a trend flattening at LLM pressures like our predictions, although in a restricted range of values (0.35–0.16 *versus* 0.69–0.16). Taking into account that we modelled the Fe/Mg exchange/equilibration neglecting the *reservoir*'s energetics, the general consistency between the present results and previous determinations suggests that iron always prefers Fe-periclase in comparison to all the other iron-bearing phases of the lower mantle.

6. CONCLUSIONS

To our knowledge, this is the first investigation which uses Gibbs energy of mixing, forward–backward transformations and treats the (Mg,Fe)O system as an open exchanger of matter with the lower mantle surroundings.

Un-mixings over the closed MgO-FeO binary at lower mantle *P-T* conditions are predicted to occur between 23 and 42 GPa in the case of LS, only. Taking into account that HS is the preferred spin state of iron up to ~ 40 GPa and that it excludes occurrence of disproportionation at any pressure, un-mixing processes are therefore unlikely. In this light, it is difficult to ascribe to un-mixing phenomena the observed compositional variability of lower mantle Fe-periclase in diamond inclusions and in H*P*-H*T* synthesis products.

In turn, using a geochemically open model and equilibrium reactions formalism, we show that the (Mg,Fe)O-system is able to continuously exchange iron with the lower mantle *reservoir* (*i.e.* MSF-system) and provides the phases $x0$ (reference average; 0.175 FeO), $x1$ and $x2$. $x1$ increases progressively in phase proportion, becoming richer and richer in iron up to 0.5 FeO at ~80 GPa (~2000 km depth). $x2$, 0.10 FeO, is *quasi*-invariant in composition and occurs with phase proportion values that decrease as a function of *P*, similarly to $x0$'s. Above ~80 GPa, such phases change neither in composition nor in phase proportion, and the Fe-rich phase becomes the most abundant in the LLM region, in terms of 0.7 phase proportion.

The resulting phases yield a larger and larger density inhomogeneity, estimated by $\Delta\rho = [\rho_{x1}-(\rho_{x0} + \rho_{x2}) \times 0.5]$. $\Delta\rho$ changes from 0.8, at 24 GPa, to 1.4, at 130 GPa, and corresponds altogether to a mean increase of approximately 10%.

The Fe/Mg partitioning between *reservoir* (roughly approximated by a "virtual" bridgmanite chemical composition) and Fe-periclase, *i.e.* Kd, decreases in LM following its geotherm, but it becomes *quasi*-constant in LLM. In fact, Kd varies from 0.64, at 24 GPa, to 0.19, at 80 GPa and from 0.18, at ~ 90 GPa, to 0.16, at 130 GPa, in general agreement with previous theoretical and experimental determinations in the case of actual bridgmanite and Fe-periclase. This suggests that iron prefers Fe-periclase in comparison to all the other iron-bearing phases of the lower mantle.

In summary:

the obtained results indicate the (Mg,Fe)O-system stabilises phases that ultimately give rise to geochemical heterogeneities as a function of the *P-T* paths in LM and LLM. Such heterogeneities are due to changes of the (Mg,Fe)O-phases in (i) composition, (ii) phase proportions, (iii) density and (iv) Fe/Mg partitioning coefficients between *reservoir* and Fe-periclase. These changes, which rapidly occur across LM, become significantly more modest in LLM, where a steady Fe-rich–phase is dominant (~0.7 phase proportion);

Fe-periclase behaves as the main "pivot" in the Fe/Mg-exchange processes with respect to the lower mantle *reservoir*;

(Mg,Fe)O is a source of geochemical heterogeneities (the average compositions from 24 to 130 GPa are strewn over the interval 0.19–0.40 FeO), but it does not give rise to any sharp discontinuity. In this view, anomalies, like the ultra-low velocity zones (ULVZs), interpreted as due to local abrupt change of density, do not seem primarily associated to the mixing behaviour of Fe-periclase.

ACKNOWLEDGEMENTS

The present research was funded by the Italian University and Research Ministry (MIUR)/PRIN2015_ project (CB). The authors are thankful to three anonymous reviewers and the Associate Editor for their useful suggestions and remarks, which relevantly improved the original manuscript.

APPENDIX A

A.1. Derivation of Eqs. (8.a) and (8.b)

Starting from Eq. (7), we require that the conservation of mass principle is fulfilled between right-hand side and left-hand side members. Therefore, we have

$$x0 = y1 \times x1 + y2 \times x2 \quad \text{(I.a.1)}$$

$$1 - x0 = y1 \times (1 - x1) + y2 \times (1 - x2). \quad \text{(I.a.2)}$$

Summing (I.a.1) and (I.a.2), we obtain

$$y1 + y2 = 1. \quad \text{(I.b)}$$

Expressing $y2$ in (I.a.1) by (I.b), we determine $y1$ as a function of $x1$ and $x2$, *i.e.* equation (8.a). Eq. (8.b) is a consequence of (I.b).

APPENDIX B

B.1. Open *system* and constrained phase assemblages

With μ_j^α and n_j^α we represent the chemical potential and number of moles of the *j*th-component with respect to the α-phase, respectively. We assume the existence of one *independent* and *known* phase, "^{0}phase". Its composition is fixed and expressed by n_j^0; ξ stands for the number of moles of the ^{0}phase. The introduction of the ^{0}phase is needed when the complexity of a system is so high that a further constraint on the nature of the involved phases can help addressing the problem. For instance, such a situation is met when transformation kinetics is low, or impaired, and leads to the persistence of one or more phases, which constrain the phase composition of the resulting assemblage. Phases other than the ^{0}phase (they are here addressed to as *dependent* phases) are in total *p*; *c* indicates the number of components.

The Gibbs energy of such a system is

$$G = \sum_{\alpha=1,p}\sum_{j=1,c} n_j^\alpha \mu_j^\alpha + \xi \sum_{j=1,c} n_j^0 \mu_j^0.$$

At given *P*-*T* conditions we have

$$dG = \sum_{\alpha=1,p}\sum_{j=1,c} \mu_j^\alpha dn_j^\alpha + \sum_{j=1,c} n_j^0 \mu_j^0 d\xi, \quad \text{(II.a)}$$

and at equilibrium $dG = 0$. If we assume the conservation of mass principle for components, *i.e.* closed system, then *c*-constraints are required to be fulfilled, *i.e.*

$$\sum_{\alpha=1,p} dn_j^\alpha + n_j^0 d\xi = 0. \quad \text{(II.b)}$$

Using the Lagrange multipliers (ψ_j) method, we combine (II.a) and (II.b), so that

$$\sum_{\alpha=1,p}\sum_{j=1,c} \mu_j^\alpha dn_j^\alpha + \sum_{j=1,c} n_j^0 \mu_j^0 d\xi + \sum_{j=1,c} \psi_j \left(\sum_{\alpha=1,p} dn_j^\alpha + n_j^0 d\xi \right) = 0.$$

Rearranging the terms of the equation above, we can write

$$\sum_{j=1,c} \left[\sum_{\alpha=1,p} (\mu_j^\alpha + \psi_j) dn_j^\alpha + (\mu_j^0 + \psi_j) n_j^0 d\xi \right] = 0. \quad \text{(II.c)}$$

(II.c) requires that

$$\mu_1^1 = \mu_1^2 = \ldots = -\psi_1 = \mu_1^0 \quad \text{(II.d)}$$
$$\mu_c^1 = \mu_c^2 = \ldots = -\psi_c = \mu_c^0$$

The set of Eq. (II.d) leads to the well understood equality between chemical potentials of the same component in different phases.

In the general approach, there is not any imposed ^{0}-phase, hence we set it aside for the moment. A set of $c \times p$ unknown $\{x_j^\alpha\}$-values, *i.e.* component fractions on which the chemical potentials depend, must be determined. In this way, the problem of the absolute amount of each component can be avoided. However, component fractions require more *p*-constraints of normalization, *i.e.* $\Sigma_{j=1,c}\, x_j^\alpha = 1$, in addition to the $c \times (p\text{-}1)$ constraints due to (II.d). Hence, at given *P* and *T*, the classic relationship: $f_{\text{degrees of freedom}} = (p \times c)\text{-}c \times (p-1)\text{-}p = c\text{-}p$ is obtained.

In the case of the presence of an *independent* ^{0}phase, the constraining equations of (II.d)-type are $p \times c$, given that the lagrangian multipliers are determined by μ_j^0, *i.e.* $-\psi_j = -\mu_j^0$. We now assume the system to be off equilibrium and, in order to evolve towards the equilibrium state, it exchanges matter with a *reservoir* according to an irreversible transformation, $dG_{irrev} < 0$, until equilibration is accomplished and $dG = 0$. Hence, the *p dependent* phases behave as an "*open system*" in the equilibration process. Relaxing the constraint of conservation of mass, we have to seek for $c \times p$ unknown $\{n_j^\alpha\}$-values, $n_j^\alpha \geq 0$, to fulfill the $c \times p$ constraint equations of (II.d)-type. In this view, the problem is solvable and the solution is unique, there being as many variables as constraints, and the independent ^{0}phase pivots equilibration of the *p dependent* phases.

We now aim to introduce more than one *independent* phase: p_{indep}-phases. First, they must be at equilibrium with each other at *P*-*T*, namely they must satisfy the constraints of the Gibbs rule, *i.e.* $p_{indep} \leq c$ and the equality of the chemical potentials. The ψ_i's, determined by the chemical potentials of the *independent* phases accordingly, lead to the $c \times p$ constraining equations of (II.d)-type. The $c \times p$ $\{n_j^\alpha\}$-values that give the *p dependent* phases are determined, and an exchange of matter between *system* and *reservoir* takes place, as in the case of the ^{0}phase.

It is worth noting that the obtained assemblage represents the least Gibbs energy system compatible with p_{indep} *independent* ($p_{indep} \leq c$) and *p dependent* phases. The assemblage of *dependent* phases, in turn, must be as physically consistent as possible with the conditions following a relaxation of the constraints of the imposed *independent* phases. In this view, $p \leq c$, for the *dependent* phases, too.

The application discussed in the text for Fe-periclase can be likened to the case in which the ubiquitous *x*0-phase acts as an *independent* ^{0}phase, whereas *x*1 and *x*2 are two *dependent* phases. In other words, the *system* is divided into two sub-*systems* (either fully consistent with the Gibbs rule) one of which exchanges matter with a *reservoir* and in this way equilibration is achieved.

APPENDIX C

C.1. System (Fe-periclase) and reservoir

The *reservoir* provides a simplified description of that portion of the lower mantle other than (Mg,Fe)O. Let us suppose that at given *P*-*T*-conditions, *reservoir* and (Mg,Fe)O, with compositions $X_{reservoir}$ and $X_{(MgFe)O}$, respectively, interact and exchange matter. If *P* and *T* are kept constant, the *system* and the *reservoir* undergo an irreversible transformation towards a Gibbs energy minimum. If the *reservoir* is *compositionally* likened to a fictitious "bridgmanite", $(Mg,Fe)SiO_3$, we can envisage an exchange of matter between it and the *system* through the following reaction:

$$(Mg_{1-x}Fe_x)O + (Mg_{1-y}Fe_y)SiO_3 \Longleftrightarrow (Mg_{1-x-\chi}Fe_{x+\chi})O + (Mg_{1-y+\chi}Fe_{y-\chi})SiO_3,$$

in which χ FeO is transferred from the *reservoir* to the Fe-periclase, and χ MgO does the opposite.

The Gibbs energy of the *reservoir* at *P-T* conditions composed by *N*-moles of a given chemical component, is represented by $G_R(P,T,N) \pm \Delta_f$; where Δ_f is the *reservoir*'s fluctuation that accounts for the energy, complex transformations, reactions, and flows of matter that take place in the lower mantle. For simplicity, we restrict to one chemical component our analysis and use $g_{Sys}(P,T,n)$ to refer to the "instantaneous" Gibbs energy of a *system* (Fe-periclase), in which *n* defines a generic reference composition at *P-T*. "Instantaneous" Gibbs energy means the Gibbs energy of the *system* frozen off equilibrium. We take $G_R(P,T,N) \gg g_{Sys}(P,T,n)$ and their total Gibbs energy is

$$G_{tot}(P,T,N,n) = g_{Sys}(P,T,n) + G_R(P,T,N) \mp \Delta_f \qquad \text{(III.a)}$$

At a given time, *system* and *reservoir* start to interact and exchange matter. The exchange of matter leads to

$$G_R(P,T,N-\chi) \mp \Delta_f$$

and

$$g_{Sys}(P,T,n+\chi).$$

From Eq. (III.a), we aim at minimizing the following quantity, with respect to χ,

$$\Delta_{tot} = G_{tot}(P,T,N-\chi,n+\chi) - G_{tot}(P,T,N,n) \mp \Delta_f \qquad \text{(III.b)}$$

in which *system* + *reservoir* evolve through an irreversible change towards an equilibrium state. Given that $|G_R(P,T,N\text{-}\chi) - G_R(P,T,N)| \ll \Delta_f$, owing to $\chi \ll N$ and, from statistical mechanics, $\Delta_f \propto N^{1/2}$, then we can neglect the change of the *reservoir*'s Gibbs energy due to an exchange of matter with the *system* with respect to the fluctuations' contribution.

In this light, Eq. (III.b) becomes

$$\Delta_{tot} \approx [\mp\Delta_f]_{reservoir} + [-\mu(P,T,n+\chi)_{Sys} \cdot \chi + O_{Sys}(\chi^2)]_{system}, \qquad \text{(III.c)}$$

Eq. (III.c) shows that if a super-*system* composed by *reservoir*+*system* is considered, then the *system* alone can be considered, if its size is significantly smaller than the *resorvoir*'s. Therefore, exchanges of matter are mainly governed by the *system*, given that they do not affect the *reservoir* more than its fluctuations do.

REFERENCES

Albarede F. and van der Hilst R. D. (2002) Zoned mantle convection. *Philos. Trans. Roy. Soc. Lond. Ser. A, Math. Phys. Eng. Sci.* **360**, 2569–2592. http://dx.doi.org/10.1098/rsta.2002.1081.

Alfredsson M., Price G. D., Catlow C. R. A., Parker S. C., Orlando R. and Brodholt J. P. (2004) Electronic structure of the antiferromagnetic B1-structured FeO. *Phys. Rev. B* **70**, 165111–165116.

Andrault D., Bolfan-Casanova N., Lo Nigro G., Bouhifd M. A., Garbarino G. and Mezouar M. (2011) Solidus and liquidus profiles of chondritic mantle: Implication for melting of the Earth across its history. *Earth Planet. Sci. Lett.* **304**, 251–259.

Autschbach J. and Srebro M. (2014) Delocalization error and "Functional Tuning" in Kohn-Sham calculations of molecular properties. *Acc. Chem. Res.* **47**, 2592–2602.

Auzende A. L., Badro J., Ryerson F. J., Weber P., Fallon S., Addad A., Siebert J. and Fiquet G. (2008) Element partitioning between magnesium silicate perovskite and ferropericlase: new insights into bulk lower-mantle geochemistry. *Earth Planet. Sci. Lett.* **269**, 164–174.

Badro J., Fiquet G., Guyot F., Rueff J., Struzhkin V. V., Vankò G. and nad Monaco G. (2003) Iron partitioning in earth's mantle: toward a deep lower mantle discontinuity. *Science* **300**, 789–791.

Barnard R. W., Dahlquist G., Pearce K., Reichel L. and Richards K. C. (1998) Gram polynomials and the Kummer function. *J. Approx. Theory* **94**, 128–143.

Belmonte D., Ottonello G. and Vetuschi Zuccolini M. (2014) Ab initio thermodynamic and thermophysical properties of sapphirine end-members in the join $Mg_4Al_8Si_2O_{20}$ – $Mg_3Al_{10}SiO_{20}$. *Am. Mineral.* **99**, 1449–1461.

Causà M., Dovesi R., Pisani C. and Roetti C. (1986) Electronic structure and stability of different crystal phases of magnesium oxide. *Phys. Rev. B* **33**, 1308–1316.

Cordier P., Amodeo J. and Carrez P. (2012) Modelling the rheology of MgO under Earth's mantle pressure, temperature and strain rates. *Nature* **481**, 177–180.

da Silva C. R. S., Wentzcovitch R. M., Patel A., Price G. D. and Karato S. I. (2000) The composition and geotherm of the lower mantle: constraints from the elasticity of silicate perovskite. *Phys. Earth Planet. Int.* **118**, 103–109.

de Koker N. (2010) Thermal conductivity of MgO periclase at high pressure: Implications for the D″ region. *Earth Planet. Sci. Lett.* **292**, 392–398.

de Wit R. W. L. and Trampert J. (2015) Robust constraints on average radial lower mantle anisotropy and consequences for composition and texture. *Earth Planet. Sci. Lett.* **429**, 101–109.

Deschamps F. and Trampert J. (2004) Towards a lower mantle reference temperature and composition. *Earth Planet. Sci. Lett.* **222**, 161–175. http://dx.doi.org/10.1016/j.epsl.2004.02.024.

Dill K. A., Bromberg S. and Stigter D. (2003) *Molecular Driving Forces: Statistical Thermodynamics in Chemistry and Biology*, first ed. Garland Science, New York.

Dobson D. P. and Brodholt J. P. (2005) Subducted banded iron formations as a source of ultralow-velocity zones at the core–mantle boundary. *Nature* **434**, 371–374.

Dovesi R., Saunders V. R., Roetti C., Orlando R., Zicovich-Wilson C. M. and Pascale F. Civalleri., et al. (2009) *CRYSTAL09 User's Manual*. University of Torino, IT, Torino.

Dubrovinsky L. S., Dubrovinskaia N. A., Saxena S. K., Annersten H., Hålenius E., Harryson H., Tutti F., Rekh S. and Le Bihan T. (2000) Stability of ferropericlase in the lower mantle. *Science* **289**, 430–432.

Dubrovinsky L. S., Dubrovinskaia N. A., Annersten H., Hålenius E. and Harryson H. (2001) Stability of magnesiowüstites $(Mg_{0.50}Fe_{0.50})O$ and $(Mg_{0.80}Fe_{0.20})O$ in the lower mantle. *Eur. J. Miner.* **113**, 857–861.

Dziewonski A. and Anderson D. L. (1981) Preliminary earth reference model. *Phys. Earth Planet. Inter.* **25**, 297–356.

Fei Y., Mao H. K., Shu J. and Hu J. (1992) P-V-T equation of state of magnesiowüstite $(Mg_{0.6}Fe_{0.4})O$. *Phys. Chem. Miner.* **18**, 416–422.

Fei W., Zhang L., Corgna A., Watson H., Ricolleau A., Meng Y. and Prakapenka V. (2007) Spin transition and equation of state of (Mg, Fe)O solid solutions. *Geophys. Res. Lett.* **34**, L17307.

Frost D. J. and Myhill R. (2016). Chemistry of the lower mantle. In Deep Earth: Physics and Chemistry of the lower mantle and core, Geophysical Monograph 217 (eds. H. Teresaki and R.A.

Fischer). American Geophysical Union. John Wiley and Sons, Inc. pp. 225–240.

Gale J. D. (1997) GULP-a computer program for the symmetry adapted simulation of solids. *JCS Faraday Trans.* **93**, 629–637.

Garnero E. J. (2004) A new paradigm for Earth's core-mantle boundary. *Science* **304**, 834–836. http://dx.doi.org/10.1126/science.1097849.

Girard J., Amulel G., Farla R., Mohiuddin A. and Karato S. (2016) Shear deformation of bridgmanite and magnesiowüstite aggregates at lower mantle conditions. *Science* **351**, 144–147.

Harte B. (2010) Diamond formation in the deep mantle; the record of mineral inclusions and their distribution in relation to mantle dehydration zones. *Mineral. Mag.* **74**, 189–215. http://dx.doi.org/10.1180/minmag.2010.074.2.189.

Irifune T., Shinmei T., McCammon C. A., Miyajima N., Rubie D. C. and Frost D. J. (2010) Iron partitioning and density changes of Pyrolite in Earth's Lower Mantle. *Science* **327**, 193–195.

Jackson I. (1998) Elasticity, composition and the temperature of the Earth's lower mantle: a reappraisal. *Geophys. J. Int.* **134**, 291–311.

Jackson J. M., Sinogeikin S. V., Jacobsen S. D., Reichmann H. J., Mackwell S. J. and Bass J. D. (2006) Single-crystal elasticity and sound velocities of $(Mg_{0.94}Fe_{0.06})O$ ferropericlase to 20 GPa. *J. Geophys. Res.* **111**, B09203.

Jacobsen S. D., Spetzler H., Reichmann H. J. and Smyth J. R. (2004) Shear waves in the diamond-anvil cell reveal pressure-induced instability in (Mg, Fe)O. *PNAS* **101**, 5867–5871.

Javoy M., Kaminski E., Guyot F., Andrault D., Sanlou J. R., Moreira M., Labrosse S., Jambon A., Agrinier P., Davaille A. and Jaupart C. (2010) The chemical composition of the Earth: Enstatite chondrite models. *Earth Planet. Sci. Lett.* **293**, 259–268.

Kaminsky F. and Lin J-F. (2017). Iron partitioning in natural lower-mantle minerals: toward a chemically heterogeneous lower mantle. Am. Miner.: http://dx.doi.org/10.2138/am-2017-5949.

Kaminsky F. (2012) Mineralogy of the lower mantle: a review of 'super-deep' mineral inclusions in diamond. *Earth Sci. Rev.* **110**, 127–147.

Kaneshima S. and Helffrich G. (1999) Dipping low-velocity layer in the mid-lower mantle: evidence for geochemical heterogeneity. *Science* **283**, 1888–1891.

Karki B. B., Wentzcovitch R. M., de Gironcoli S. and Baroni S. (2001) First principles thermoelasticity of $MgSiO_3$-perovskite: consequences for the inferred properties of the lower Mantle. *Geophys. Res. Lett.* **28**, 2699–3702.

Kennett B. L., Engdahl E. R. and Buland R. (1995) Constraints on seismic velocities in the earth from travel times. *Geophys. J. Int.* **122**, 108–124.

Kobayashi Y., Kondo T., Ohtani E., Hirao N., Miyajima N., Yagi T., Nagase T. and Kikegawa T. (2005) Fe-Mg partitioning between (Mg, Fe)SiO_3 post-perovskite, perovskite, and magnesiowüstite in the Earth's lower mantle. *Geophys. Res. Lett.* **32**, L19301. http://dx.doi.org/10.1029/ 2005GL023257.

Kung J., Li B., Weidner D. J., Zhang J. and Liebermann R. C. (2002) Elasticity of (Mg0.83, Fe0.17)O ferropericlase at high pressure: Ultrasonic measurements in conjunction with X-radiation techniques. *Earth Planet. Sci. Lett.* **203**, 557–566.

Kurnosov A., Marquardt H., Frost D. J., Boffa Ballaran T. and Ziberna L. (2017) Evidence for a F3+-rich pyrolytic lower mantle from (Al, Fe)-bearing bridgmanite elasticity data. *Nature* **543**, 543–546.

Lay T. and Helmberger D. V. (1983) A shear velocity discontinuity in the lower mantle. *Geoph. Res. Lett.* **10**, 63–66.

Lay T., Garner E. J. and Williams Q. (2004) Partial melting in a thermo-chemical boundary layer at the base of the mantle. *Phys. Earth Planet. Inter.* **146**, 441–467.

Lewis G. V. and Catlow C. R. A. (1985) Potential models for ionic oxides. *J. Phys. C: Solid State Phys.* **18**, 1149–1162.

Li L., Brodholt J. P., Stackhouse S., Weidner D. J., Alfredsson M. and Price G. D. (2005) Elasticity of (Mg, Fe)(Si, Al)O_3 perovskite a high pressure. *Earth Planet. Sci. Lett.* **240**, 529–536. http://dx.doi.org/10.1016/j.epsl.2005.09.030.

Lin J. F., Heinz D. L., Ma H., Hemley R. J., Devine J. M., Li J. and Shen G. (2003) Stability of magnesiowüstite in Earth's lower mantle. *PNAS* **100**, 4405–4408.

Lin J. F., Vankò G., Jacobsen S. D., Iota V., Struzhkin V. V., Prakapenka V. B., Kuznetsov A. and Yoo C. S. (2007) Spin transition zone in Earth's lower mantle. *Science* **317**, 1740–1743.

Lin J. F., Wenk H. R., Voltolini M., Speziale S., Shu J. and Duffy T. S. (2009) Deformation of lower-mantle ferropericlase (Mg, Fe)O across the electronic spin transition. *Phys. Chem. Miner.* **36**, 585–592.

Lin J. F., Spezial S., Ma Z. and Marquard H. (2013) Effects of the electronic spin transitions of iron in lower mantle minerals: implications for deep mantle geophysics and geochemistry. *Rev. Geophys.* **51**, 244–275.

Lyubetskaya T. and Korenaga J. (2007) Chemical composition of Earth's primitive mantle and its variance: 1. Method and results. *J. Geophys. Res.* **112**, B03211. http://dx.doi.org/10.1029/2005JB004223.

Lyubutin S., Gavriliuk A. G., Frolov K. V., Lin J. F. and Troyan I. A. (2009) High_Spin–Low_Spin Transition in Magnesiowüstite (Mg0.75, Fe0.25)O at High Pressures under Hydrostatic Conditions. *JETP Lett.* **90**, 617–622.

Madi K., Forest S., Cordier P. and Boussuge M. (2005) Numerical study of creep in two-phase aggregates with a large rheology contrast: implications for the lower mantle. *Earth Planet. Sci. Lett.* **237**, 223–238.

Mainprice D. (2007). Seismic Anisotropy of the deep Earth from a Mineral and Rock Physics Perspective. In Treatise on Geophysics, vol. 2 (ed G. Schubert). Elsevier. pp. 437–491.

Mao W. L., Mao H. K., Sturhahn W., Zhao J. Y., Prakapenka V. B., Meng Y., Shu J. F., Fei Y. W. and Hemley R. J. (2006) Iron-rich post-perovskite and the origin of ultralow-velocity zones. *Science* **312**, 564–565.

Matas J., Bass J., Ricard Y., Mattern E. and Bukowinski MST. (2007) On the bulk composition of the lower mantle: predictions and limitations from generalized inversion of radial seismic profiles. *Geophys. J. Int.* **170**, 764–780.

Mattern E., Matas J., Ricard Y. and Bass J. D. (2005) Lower mantle composition and temperature from mineral physics and thermodynamic modelling. *Geophys. J. Int.* **160**, 973–990.

McDonough W. F. and Sun S. (1995) The composition of the Earth. *Chem. Geol.* **120**, 223–253. http://dx.doi.org/10.1016/0009-2541(94)00140-4.

McNamara A. K., Garnero E. J. and Rost S. (2010) Tracking deep mantle reservoirs with ultra-low velocity zones. *Earth Planet. Sci. Lett.* **299**, 1–9. http://dx.doi.org/10.1016/j.epsl.2010.07.042.

Merli M., Sciascia L., Pavese A. and Diella V. (2015) Modelling of thermo-chemical properties over the subsolidus MgO–FeO binary, as a function of iron spin configuration, composition and temperature. *Phys. Chem. Min.* **42**, 347–362.

Merli M., Bonadiman C., Diella V. and Pavese A. (2016) Lower mantle hydrogen partitioning between periclase and perovskite: a quantum chemical modelling. *Geochim. Cosmochim. Acta* **173**, 304–318.

Miyajima Y., Ueda T., Adachi H., Fujii T., Onaka S. and Kato M. (2014) Dislocation density of FCC metals processed by ARB.

6th International Conference on nanomaterials by severe plastic deformation. IOP Conf. Series: Materials Science and Engineering, vol. 63, 012138. http://dx.doi.org/10.1088/1757-899X/63/1/012138.

Miyajima N., Yagi T., Hirose K., Kondo T., Kiyoshi Fujino K. and Miura H. (2001) Potential host phase of aluminium and potassium in the Earth's lower mantle. *Am. Mineral.* **86**, 740–746.

Muir J. and Brodholt J. (2015) Elastic properties of ferropericlase at lower mantle conditions and its relevance to ULVZs. *Earth Planet. Sci. Lett.* **417**, 40–48.

Murakami M., Hirose K., Sata N. and Ohishi Y. (2005) Post-perovskite phase transition and mineral chemistry in the pyrolitic lowermost mantle. *Geophys. Res. Lett.* **32**, L03304. http://dx.doi.org/10.1029/2004GL021956.

Murakami M., Ohishi Y., Hirao N. and Hirose K. (2012) A perovskitic lower mantle inferred from high-pressure, high-temperature sound velocity data. *Nature* **485**, 90–94. http://dx.doi.org/10.1038/nature11004.

Nakajima Y., Frost D. J. and Rubie D. C. (2012) Ferrous iron partitioning between magnesium silicate perovskite and ferropericlase and the composition of perovskite in the Earth's lower mantle. *J Geophys. Res.* **117**, B08201. http://dx.doi.org/10.1029/2012JB009151.

Narygina O., Dubrovinsky L., Samuel H., McCammon C., Kantor I., Glazyrin I., Pascarelli S., Aquilanti G. and Prakapenka V. (2011) Chemically homogeneous spin transition zone in Earth's lower mantle. *Phys. Earth Planet. Inter.* **185**, 107–111.

Nomura R., Ozawa H., Tateno S., Hirose K., Hernlund J., Muto S., Ishii H. and Hiraoka N. (2011) Spin crossover and iron-rich silicate melt in the Earth's deep mantle. *Nature* **473**, 199–202.

Ono S. (2008) Experimental constraints on the temperature profile in the lower mantle. *Phys. Earth Planet. Inter.* **170**, 267–273. http://dx.doi.org/10.1016/j.pepi.2008.06.033.

Ono S. and Oganov A. R. (2005) In situ observations of phase transition between perovskite and $CaIrO_3$-type phase in $MgSiO_3$ and pyrolitic mantle composition. *Earth Planet. Sci. Lett.* **236**, 914–932.

Ohta K., Fujino K., Kuwayama Y., Kondo T., Shimizu K. and Ohishi Y. (2014) Highly conductive iron-rich (Mg, Fe)O magnesiowüstite and its stability in the Earth's lower mantle. *J. Geophys. Res. Solid Earth* **119**, 4656–4665. http://dx.doi.org/10.1002/ 2014JB010972.

Otsuka K., McCammon C. A. and Karato S. (2010) Tetrahedral occupancy of ferric iron in (Mg, Fe)O: implications for point defects in the Earth's lower mantle. *Phys. Earth Plan. Int.* **180**, 179–188.

Ottonello G., Civalleri B., Ganguly J., Perger W. F., Belmonte D. and Vetuschi Zuccolini M. (2010) Thermo-chemical and thermo-physical properties of the high pressure phase Anhydrous B ($Mg_{14}Si_5O_{24}$): an ab initio all-electron investigation. *Am. Mineral.* **95**, 563–573.

Ottonello G. (1997) *Principles of Geochemistry*. Columbia University Press, New York.

Pamato M. G., Kurnosov A., Boffa Ballaran T., Trots D.M. Caracas R. and Frost DJ. (2014) Chemistry and Mineralogy of Earth's Mantle. Hexagonal $Na_{0.41}[Na_{0.125}Mg_{0.79}Al_{0.085}]_2[Al_{0.79}Si_{0.21}]_6O_{12}$ (NAL phase): Crystal structure refinement and elasticity. *Am. Mineral.* **99**, 1562–1569.

Paktunc A. D. (1998) MODAN: an interactive computer program for estimating mineral quantities based on bulk composition. *Comput. Geosci.* **22**, 425–431.

Prescher C., Langenhorst F., Dubrovinsky L., Prakapenka V. and Miyajima N. (2014) The effect of Fe spin crossovers on its partitioning behavior and oxidation state in a pyrolitic Earth's lower mantle system. *Earth Planet. Sci. Lett.* **399**, 86–91.

Reali R., Boioli F., Gouriet K., Carrez P., Devincre B. and Cordier P. (2017) Modelling plasticity of MgO by 2.5D dislocation dynamics simulations. *Mat. Sci. Eng. A* **690**, 52–61.

Richet P., Mao H.-K. and Bell P. M. (1989) Bulk moduli of magnesiowüstites from static compression experiments. *J. Geoph. Res.* **94**, 3037–3045.

Rost S., Garnero E. J., Williams Q. and Manga M. (2005) Seismological constraints on a possible plume root at the core–mantle boundary. *Nature* **435**, 666–669.

Sakai T., Ohtani E., Terasaki H., Sawada N., Kobayashi Y., Miyahara M., Nishijima M., Hirao N., Ohishi Y. and Kikegawa T. (2009) Fe–Mg partitioning between perovskite and ferropericlase in the lower mantle. *Am. Mineral.* **94**, 921–925.

Sanchez J. M., Ducastelle F. and Gratias D. (1984) Generalized cluster description of multicomponent systems. *Phys. A* **128**, 334–350. http://dx.doi.org/10.1016/0378-4371(84)90096-7.

Scanavino I. and Prencipe M. (2013) Ab-initio determination of high-pressure and high-temperature thermoelastic and thermodynamic properties of low-spin (Mg1–xFex)O ferropericlase with x in the range [0.06, 0.59]. *Am. Mineral.* **98**, 1270–1278.

Scanavino I., Belousov R. and Prencipe M. (2012) Ab initio quantum-mechanical study of the effects of the inclusion of iron on thermoelastic and thermodynamic properties of periclase (MgO). *Phys. Chem. Miner.* **39**, 649–663.

Sidorin I., Gurnis M. and Helmberger D. V. (1999) Evidence for a ubiquitous seismic discontinuity at the base of the mantle. *Science* **286**, 1326–1331. http://dx.doi.org/10.1126/science.286.5443.1326.

Sinmyo R. and Hirose K. (2013) Iron partitioning in pyrolitic lower mantle. *Phys. Chem. Miner.* **40**, 107–113.

Sinmyo R., Hirose K., Nishio-Hamane D., Seto Y., Fujino K., Sata N. and Ohishi Y. (2008) Partitioning of iron between perovskite/postperovskite and ferropericlase in the lower mantle. *J. Geoph. Res.* **113**, B11204. http://dx.doi.org/10.1029/2008JB005730.

Stølen S. and Grande T. (2004). Chemical Thermodynamics of Materials: Macroscopic and Microscopic Aspects. John Wiley and Sons Ltd.

Stixrude L. and Lithgow-Bertelloni C. (2007) Influence of phase transformations on lateral heterogeneity and dynamics in Earth's mantle. *Earth Planet. Sci. Lett.* **263**, 45–55.

Thorne M. S., Garnero E. J., Jahnke G., Igel H. and McNamara A. K. (2013) Mega ultra-low velocity zone and mantle flow. *Earth Planet. Sci. Lett.* **364**, 59–67. http://dx.doi.org/10.1016/j.epsl.2012.12.034.

Tommaseo C. E., Devive J., Merkel S., Speziale S. and Wenk H. R. (2006) Texture development and elastic stresses in magnesiowüstite at high pressure. *Phys. Chem. Min.* **33**, 84–97.

Trampert J., Deschamps F., Resovsky J. S. and Yuen D. A. (2004) Probabilistic tomography maps chemical heterogeneities throughout the lower mantle. *Science* **306**, 853–856. http://dx.doi.org/10.1126/science.1101996.

Valerio G., Catti M., Dovesi R. and Orlando R. (1995) Ab initio study of antiferromagnetic rutile-type FeF_2. *Phys. Rev. B* **52**, 2422–2427.

van Orman J. A., Fei Y., Hauri E. H. and Wang J. (2003) Diffusion in MgO at high pressures: constraints on deformation mechanisms and chemical transport at the core-mantle boundary. *J. Geophys. Res.* **30**, 1056.

van Westrenen W., Li J., Fei J., Frank M. R., Hellwig H., Komabayashi T., Mibef K., Minarik W. G., van Orman J. A., Watson H. C., Funakoshi K. and Schmidt M. W. (2005) Thermoelastic properties of $(Mg_{0.64}Fe_{0.36})O$ ferropericlase based on in situ X-ray diffraction to 26.7 GPa and 2173 K. *Phys. Earth Planet. Int.* **151**, 163–176.

Vassiliou M. S. and Ahrens T. J. (1982) The equation of state of $Mg_{0.6}Fe_{0.4}O$ to 200 GPa. *Geoph. Res. Lett.* **9**, 127–130.

Vilella K., Shim S.-H., Farnetani C. G. and Badro J. (2015) Spin state transition and partitioning of iron: Effects on mantle dynamics. *Earth Planet. Sci. Lett.* **417**, 57–66.

Wdowik U.D., Piekarz P., Jochym P.T., Parlinski K. and Olés A. M. (2015). Influence of isolated and clustered defects on electronic and dielectric properties of wüstite. Phys. Rev. B 91, 195111–1/10.

Wentzcovitch R. M., Karki B. B., Cococcioni M. and de Gironcoli S. (2004) Thermoelastic properties of $MgSiO_3$-perovskite: insights on the nature of the Earth's lower mantle. *Phys. Rev. Lett.* **92**, 018501.

Wentzcovitch R. M., Justo J. F., Wu Z., da Silva C. R. S., Yuen D. and Kohlstedt D. (2009) Anomalous compressibility of ferropericlase throughout the iron spin cross-over. *PNAS* **106**, 8447–8452.

Wicks J. K., Jackson A. and Sturhahn W. (2010) Very low sound velocities in iron-rich (Mg, Fe)O: implications for the core–mantle boundary region. *Geophys. Res. Lett.* **37**, L153041. http://dx.doi.org/10.1029/2010GL043689.

Yuge K. (2010) Cluster expansion approach for transmutative lattice systems. *J. Phys. Condens. Matter* **22**, 125402.

Zha C. S., Mao H. and Hemley R. J. (2000) Elasticity of MgO and a primary pressure scale up to 55 GPa. *PNAS* **97**, 13494–13499.

Zhang J. and Kostak P. (2002) Thermal equation of state of magnesiowüstite $(Mg_{0.6}Fe_{0.4})O$. *Phys. Earth Planet. Inter.* **129**, 301–311.

Zhang S., Cottaar S., Liu T., Stackhouse S. and Militzer B. (2016) High-pressure, temperature elasticity of Fe- and Al-bearing $MgSiO_3$: Implications for the Earth's lower mantle. *Earth Planet. Sci. Lett.* **343**, 264–273.

Associate editor: Michael J. Toplis